The measured reference value for the radius of sample P175A is 149.7±0.1mm, which agrees very closely with the values obtained both through two-dimensional and three-dimensional curve-fitting. A summary of the radius of curvature measurements obtained using different procedures throughout the data processing of the ronchigrams is presented in Table 6.2.9.

Table 6.2.9: Comparison of measured radius of curvature with the reference Möller-Wedel radioscope measurement. %Deviation refers to relative differences between the measured and reference values.

Measuring procedure	**Original Data**	**R(mm)**	**s (mm)**	**%Deviation**
2D curve-fitting	$N_X(x_S)$; non-µstepped.	149.81	0.025	0.07
	$N_Y(y_S)$; non-µstepped	149.97	0.015	0.18
	$N_X(x_S)$;µstepped	149.79	0.003	0.06
	$N_Y(y_S)$;µstepped	149.96	0.002	0.17
3D curve-fitting	Topography; non-µstepped	149.78	0.027	0.05
	Topography; µstepped	149.78	$2.4\ 10^{-3}$	0.05
Möller-Wedel radioscope		***149.7±0.1***		

Results in Table 6.2.9 show that, although two-dimensional and three-dimensional curve fitting procedures reveal similar standard deviations, three-dimensional curve fitting procedures are the ones that obtain a closer measurement to the reference values of the surface's radius of curvature with or without microstepping procedures applied. However, *both* procedures attain values very close to the reference measured value, as the maximum departure from the reference is 0.18% (1 part in 555). The value measured through three-dimensional curve-fitting procedures only departs from the reference value by 0.05% (1 part in 2000), which provides a consistent validation of the proposed technique's capacity to measure radii of curvature.

Unfortunately, no comparative data for the topography of the surface have been obtained, as the interferometric and profilometric techniques available to us could hardly handle a $204mm^2$ sample surface without sample displacements, although interesting advances in the field are being made [Laguarta 1998]. However, when reference measurements of radius of curvature were performed on the Möller-Wedel radioscope,

slight toricity could be appreciated on the surface, as two best focusing positions in orthogonal directions of the test were obtained at two different distances with the best overall focusing of the test lying at an intermediate distance between them. The total difference of radius of curvature amounted to just around 0.1mm. This slight toricity has already been observed when plotting the residuals of the reconstructed topography from the best fit sphere, in Fig.6.2.12d and Fig.6.2.13d, where the axis of a slightly toroidal surface may be observed positioned approximately along the 30° direction from the X axis.

6.3 Complete experimental results

Since the details of each measurement process have already been given, it is now time to perform a complete series of surface topographies in different positions in order to validate the measurement technique and to present its behavior under different experimental conditions. The sample surfaces to be used and the three different d_R distances where these are placed have already been presented in Table 6.1.1.

As explained in 6.2, only microstepped experiments will be presented, as non-microstepped experiments unnecessarily duplicate the amount of information provided. Differences in microstepped and non-microstepped measurements for each of the samples fully coincide with the ones described in the typical measurement example of Section 6.2: non-microstepped measurements are a quicker alternative to microstepped ones, yielding comparable radius of curvature values to those of microstepped experiments, although the former lack the intensive sampling of the measured surface provided by the latter.

For each of the samples, a table divided into three sections will be provided. The first section will contain a set of parameters of the considered experiment (the number of points N, the maximum measured height variation of the reconstructed surface and the sampled area). In the second section of the table we will show the parameters obtained along the previously described two-dimensional fitting procedures (curvatures, angular misalignment, correlation coefficients and radius along the X and Y axes). In the third section of the table, parameters obtained through three-dimensional fitting (radius of curvature, and the coordinates of the vertex of the surface), including the standard

deviation of the fit for each of the parameters are detailed. The range of height deviations from the best fit sphere, obtained by subtracting the measured data from the fitted sphere and obtaining the maximum positive and negative deviations, is also presented. The Möller-Wedel radioscopic measurement for the radius of curvature used as a reference is also provided for each sample at the foot of the table.

Going by the table of results for each of the samples, a general pseudocolor plot of the topography of the surface and of the residuals of the measured data from the best fit sphere in all the positions considered is provided. Each figure was prepared to summarize the measuring process of one sample, meaning that this contains the information about the topographies and residuals of the surface measured for that sample along the three different positions where measurements have been made. A common contour step is used in the three different positions of a given sample, and is specified at the top of each figure. In the residual plot, a blue level has been kept as a reference in order to indicate the zones of coincidence of the measured surface and the best fit sphere.

The tables and figures for the measured results will be presented in Section 6.3.1, and analyzed in Section 6.3.2.

6.3.1.- Measured data.

Table 6.3.1 and Figure 6.3.1 depict the results obtained for sample P175A.
Table 6.3.2 and Figure 6.3.2 depict the results obtained for sample P175B.
Table 6.3.3 and Figure 6.3.3 depict the results obtained for sample P200A.
Table 6.3.4 and Figure 6.3.4 depict the results obtained for sample P200B.
Table 6.3.5 and Figure 6.3.5 depict the results obtained for sample P275A.
Table 6.3.6 and Figure 6.3.6 depict the results obtained for sample P275B.

For each of the samples, positions P1, P2 and P3 are characterized by their distance from the Ronchi ruling to the surface (the aforementioned d_R distance), which has already been presented in Table 6.1.1.

In all tables, the numerical results are presented following the same notation of previous Sections, in the cases where the measured magnitudes have been already presented. So:

- N stands for the total number of data points.
- Δz stands for the total measured height range.
- A stands for the measured area.
- C_X stands for the curvature measured in the X axis direction.
- C_Y stands for the curvature measured in the Y axis direction.
- K_X stands for the angular misalignment in the X axis direction.
- K_Y stands for the angular misalignment in the cross curve direction.
- r_X^2 stands for the two-dimensional correlation quoeficient of the linear fit along the direction of the X axis.
- r_Y^2 stands for the two-dimensional correlation quoeficient of the linear fit along the direction of the Y axis.
- R_X stands for the radius of curvature measured in the X axis direction.
- R_Y stands for the radius of curvature measured in the Y axis direction.
- R stands for the radius of curvature measured through three-dimensional fitting.
- x_0 stands for the x coordinate for the position of the vertex of the surface.
- y_0 stands for the y coordinate for the position of the vertex of the surface.
- σ_α stands for the standard deviation of parameter α.
- r^2 stands for the correlation quoeficient of the three-dimensional fitting procedure.
- $\Delta z_{RESIDUAL}$ stands for the calculated range of height residuals.

This page was intentionally left blank.

Table 6.3.1: Measured numerical results for sample P175A.

Sample P175A	Parameter	P1 d_R=171.2mm	P2 d_R=177.3mm	P3 d_R=183.5mm
Experiment	N(points)	7583	11320	15646
	Δz(mm)	0.358	0.316	0.279
	A(mm^2)	203.6	193.5	183.2
2D fitting	C_X(mm^{-1})	6.676 10^{-3}	6.677 10^{-3}	6.673 10^{-3}
	K_X(rad)	-4.409 10^{-3}	-4.433 10^{-3}	-3.824 10^{-3}
	r_x^2	0.999997	0.999993	0.999992
	C_Y(mm^{-1})	6.668 10^{-3}	6.670 10^{-3}	6.664 10^{-3}
	K_Y(rad)	-2.052 10^{-3}	2.095 10^{-4}	4.423 10^{-4}
	r_Y^2	0.999999	0.999998	0.999997
	R_X(mm)	149.81	149.76	149.86
	R_Y(mm)	150.04	149.94	150.06
3D fitting	R(mm)	149.75	149.78	149.93
	σ_R(mm)	2.3 10^{-3}	2.2 10^{-3}	2.4 10^{-3}
	x_0(mm)	0.6610	0.6643	0.5735
	σ_{Xo}(mm)	4.3 10^{-5}	3.8 10^{-5}	3.8 10^{-5}
	y_0(mm)	-3.067 10^{-2}	-3.149 10^{-2}	6.744 10^{-2}
	σ_{Yo}(mm)	3.9 10^{-6}	4.9 10^{-6}	2.5 10^{-5}
	r^2	0.999998	0.999998	0.999996
	$\Delta z_{RESIDUAL}$(mm)	4.951 10^{-4}	3.353 10^{-4}	5.661 10^{-4}

Möller-Wedel radioscope reference measurement: R=149.7±0.1mm

Fig. 6.3.1: Measured surface topographies and residuals: Sample P175A.

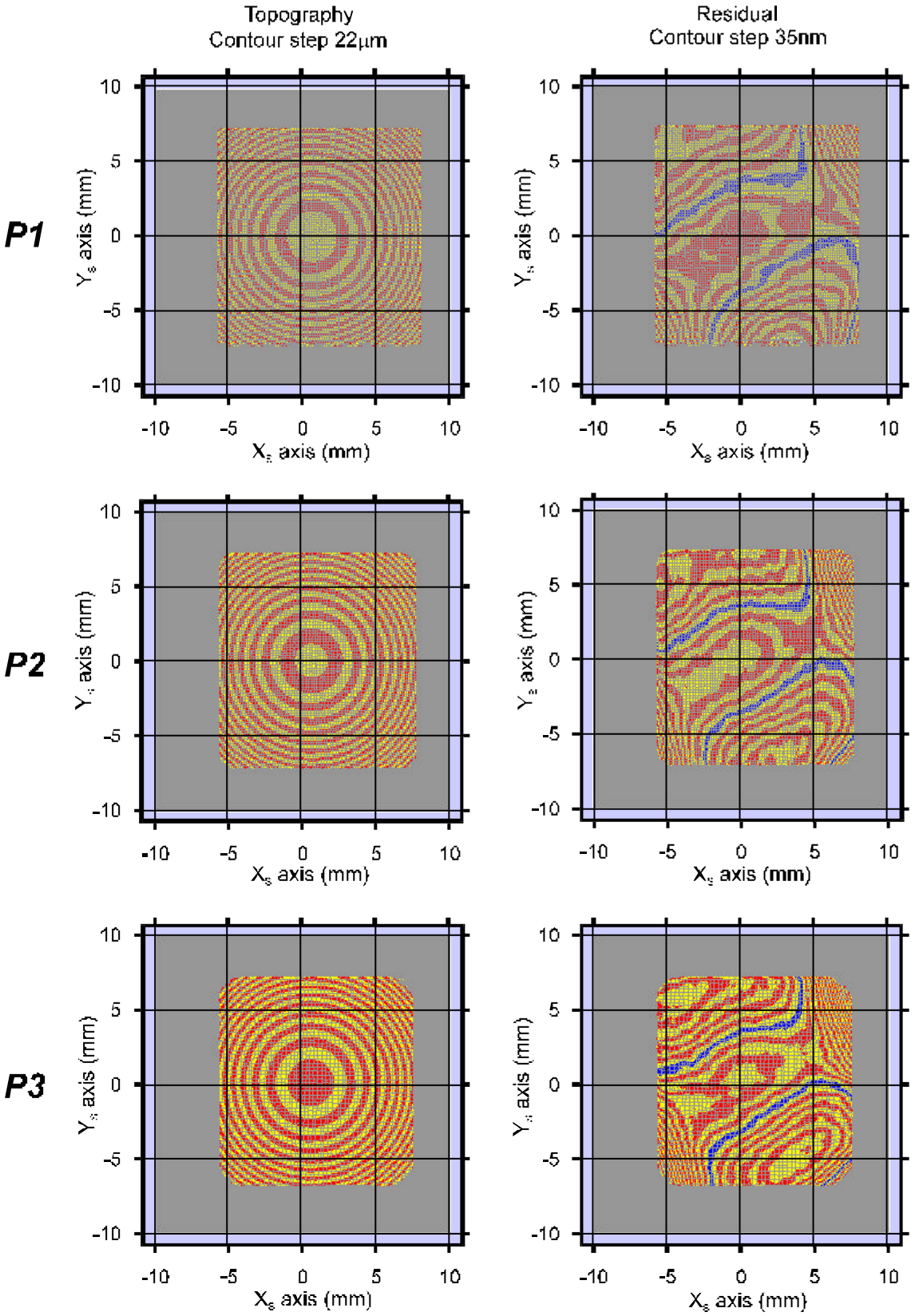

Table 6.3.2:Measured numerical results for sample P175B.

Sample P175B	Parameter	P1 d_R=171.2mm	P2 D_R=177.3mm	P3 d_R=183.5mm
Experiment	N(points)	7615	11314	15690
	Δz(mm)	0.344	0.305	0.273
	A(mm^2)	202.5	191.0	183.2
2D fitting	C_X(mm^{-1})	$6.693\ 10^{-3}$	$6.691\ 10^{-3}$	$6.682\ 10^{-3}$
	K_X(rad)	$-3.733\ 10^{-3}$	$-3.383\ 10^{-3}$	$-3.677\ 10^{-3}$
	r_x^2	0.999997	0.999996	0.999995
	C_Y(mm^{-1})	$6.665\ 10^{-3}$	$6.663\ 10^{-3}$	$6.653\ 10^{-3}$
	K_Y(rad)	$2.702\ 10^{-4}$	$5.282\ 10^{-4}$	$8.613\ 10^{-4}$
	r_Y^2	0.999998	0.999997	0.999995
	R_X(mm)	149.40	149.45	149.65
	R_Y(mm)	150.04	150.09	150.30
3D fitting	R(mm)	149.66	149.73	149.99
	σ_R(mm)	$3.8\ 10^{-3}$	$3.2\ 10^{-3}$	$3.1\ 10^{-3}$
	x_0(mm)	0.5574	0.5056	0.550
	σ_{Xo}(mm)	$6.8\ 10^{-5}$	$5.3\ 10^{-5}$	$4.9\ 10^{-5}$
	y_0(mm)	$4.089\ 10^{-2}$	$7.943\ 10^{-2}$	0.133
	σ_{Yo}(mm)	$2.9\ 10^{-5}$	$1.9\ 10^{-3}$	$1.5\ 10^{-5}$
	r^2	0.999995	0.999995	0.999994
	$\Delta z_{RESIDUAL}$(mm)	$6.330\ 10^{-4}$	$6.220\ 10^{-4}$	$6.950\ 10^{-4}$

Möller-Wedel radioscope reference measurement: R=149.8±0.1mm

Fig. 6.3.2: Measured surface topographies and residuals: sample P175B.

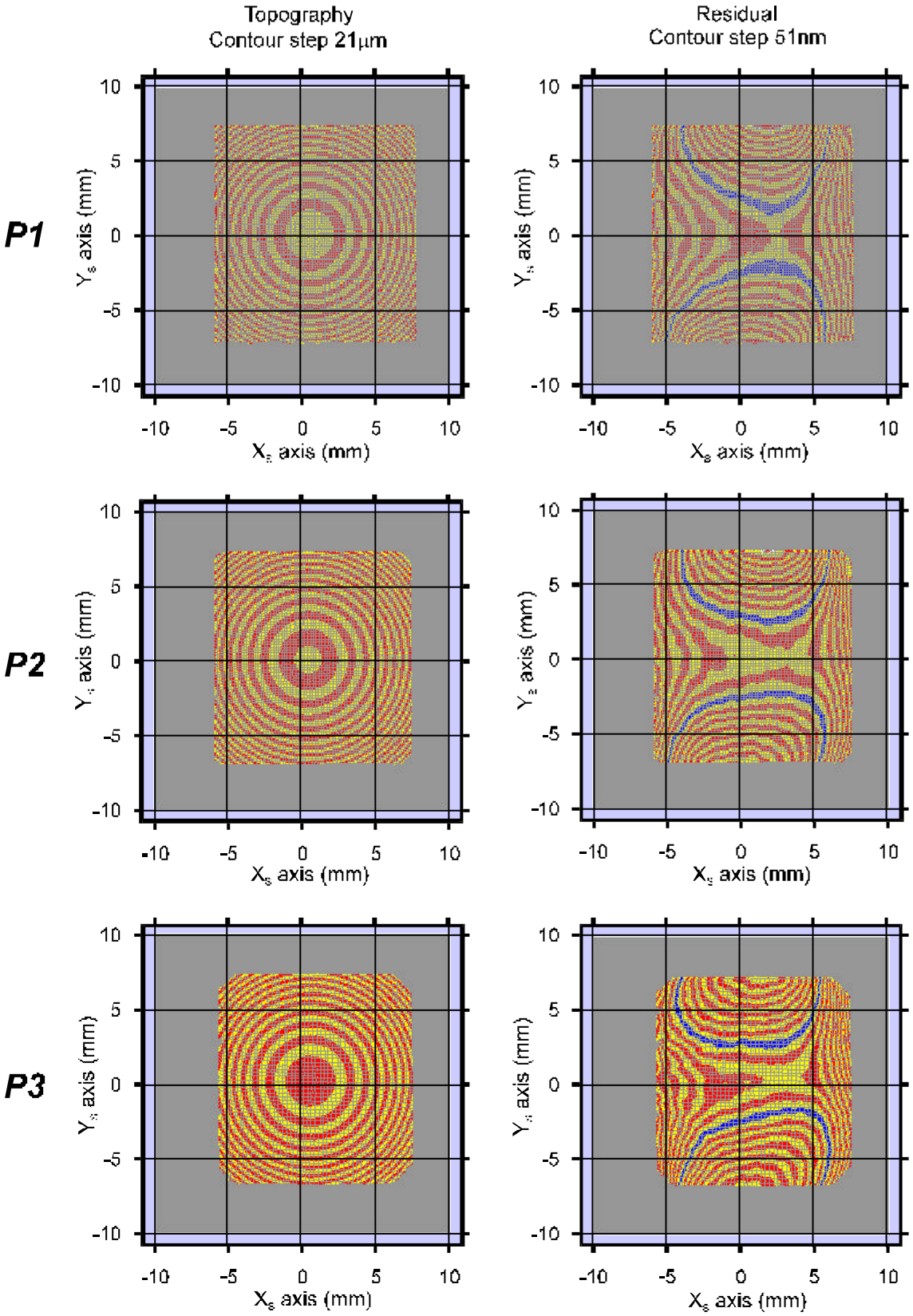

Table 6.3.3: Measured numerical results for sample P200A.

Sample P200A	Parameter	P1 d_R=181.2mm	P2 d_R=187.2mm	P3 d_R=192.9mm
Experiment	N(points)	7982	11821	15853
	Δz(mm)	0.369	0.332	0.296
	A(mm^2)	231.3	221.2	212.6
2D fitting	C_X(mm^{-1})	$6.295\ 10^{-3}$	$6.284\ 10^{-3}$	$6.278\ 10^{-3}$
	K_X(rad)	$-2.467\ 10^{-3}$	$-2.510\ 10^{-3}$	$-2.369\ 10^{-3}$
	r_x^2	0.999947	0.999997	0.999996
	C_Y(mm^{-1})	$6.272\ 10^{-3}$	$6.258\ 10^{-3}$	$6.258\ 10^{-3}$
	K_Y(rad)	$-7.308\ 10^{-4}$	$-4.613\ 10^{-4}$	$-2.491\ 10^{-4}$
	r_Y^2	0.999996	0.999994	0.999993
	R_X(mm)	158.86	159.13	159.28
	R_Y(mm)	159.45	159.59	159.80
3D fitting	R(mm)	159.16	159.33	159.55
	σ_R(mm)	$3.7\ 10^{-3}$	$3.2\ 10^{-3}$	$2.9\ 10^{-3}$
	x_0(mm)	0.1200	0.4000	0.3775
	σ_{Xo}(mm)	$6.2\ 10^{-5}$	$5.3\ 10^{-5}$	$4.6\ 10^{-5}$
	y_0(mm)	-0.3935	$7.5050\ 10^{-2}$	$4.1435\ 10^{-2}$
	σ_{Yo}(mm)	$6.1\ 10^{-5}$	$3.3\ 10^{-5}$	$3.4\ 10^{-6}$
	r^2	0.999996	0.999996	0.999995
	$\Delta z_{RESIDUAL}$(mm)	$6.866\ 10^{-4}$	$7.419\ 10^{-4}$	$6.697\ 10^{-4}$

Möller-Wedel radioscope reference measurement: R=159.3±0.1mm

Fig. 6.3.3: Measured surface topographies and residuals: sample P200A.

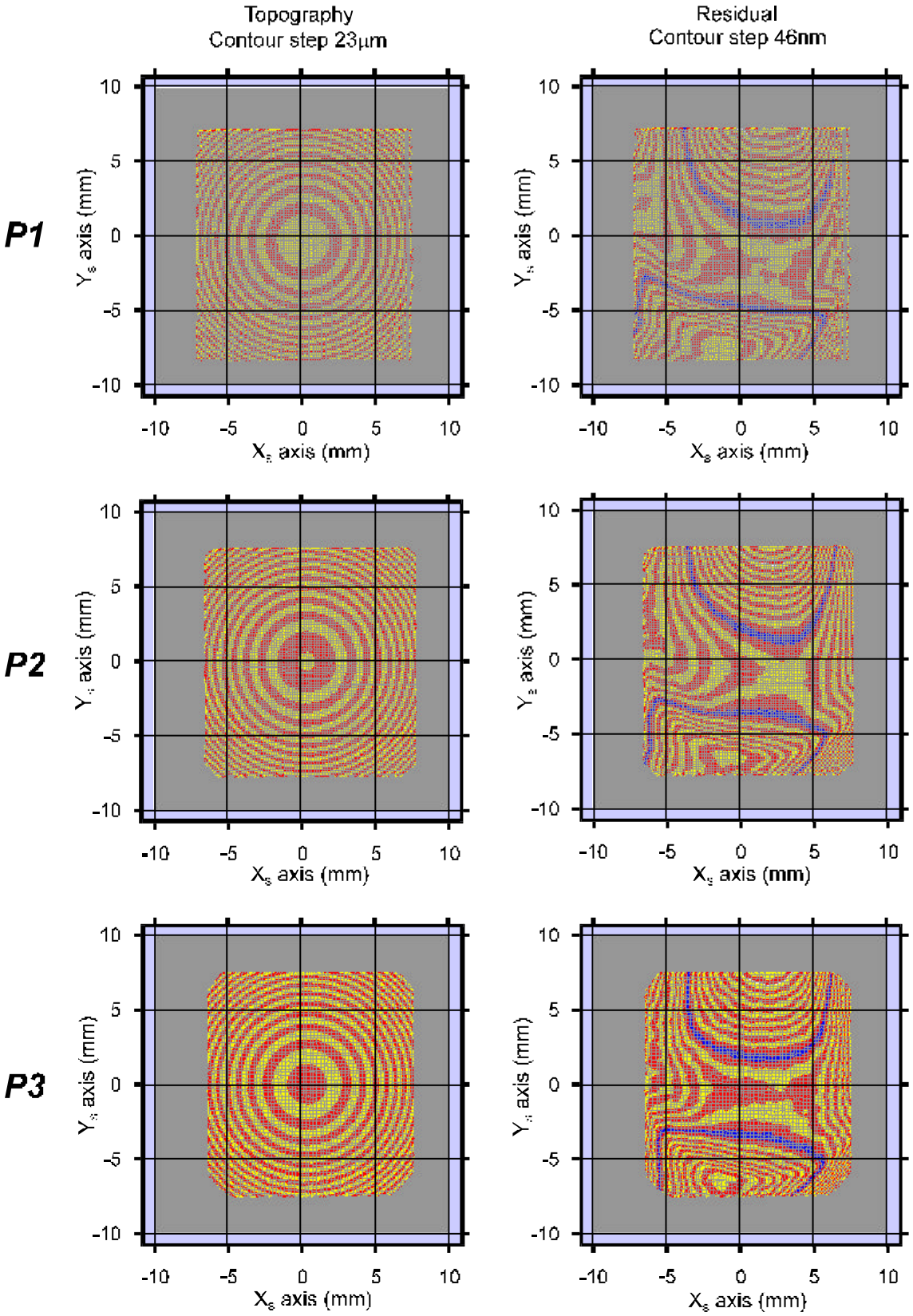

Table 6.3.4: Measured numerical results for sample P200B.

Sample P200B	Parameter	P1 d_R=181.1mm	P2 d_R=187.1mm	P3 d_R=192.8mm
Experiment	N(points)	7885	11893	15655
	Δz(mm)	0.393	0.353	0.304
	A(mm^2)	231.2	221.9	213.1
2D fitting	C_X(mm^{-1})	6.281 10^{-3}	6.278 10^{-3}	6.274 10^{-3}
	K_X(rad)	-4.718 10^{-3}	-5.184 10^{-3}	-3.730 10^{-4}
	r_x^2	0.999996	0.999995	0.999992
	C_Y(mm^{-1})	6.279 10^{-3}	6.275 10^{-3}	6.265 10^{-3}
	K_Y(rad)	-6.134 10^{-4}	-2.441 10^{-4}	-3.830 10^{-4}
	r_Y^2	0.999998	0.999997	0.999990
	R_X(mm)	159.20	159.29	159.39
	R_Y(mm)	159.27	159.37	159.61
3D fitting	R(mm)	159.12	159.26	159.46
	σ_R(mm)	2.2 10^{-3}	1.9 10^{-3}	1.92 10^{-3}
	x_0(mm)	0.751	0.826	0.595
	σ_{Xo}(mm)	3.9 10^{-5}	3.4 10^{-5}	2.6 10^{-5}
	y_0(mm)	9.784 10^{-2}	3.904 10^{-2}	6.237 10^{-2}
	σ_{Yo}(mm)	2.5 10^{-5}	9.3 10^{-6}	1.8 10^{-5}
	r^2	0.999999	0.999998	0.999998
	$\Delta z_{RESIDUAL}$(mm)	5.146 10^{-4}	4.802 10^{-4}	5.056 10^{-4}

Möller-Wedel radioscope reference measurement: R=159.4±0.1mm

Fig. 6.3.4: Measured surface topographies and residuals: sample P200B.

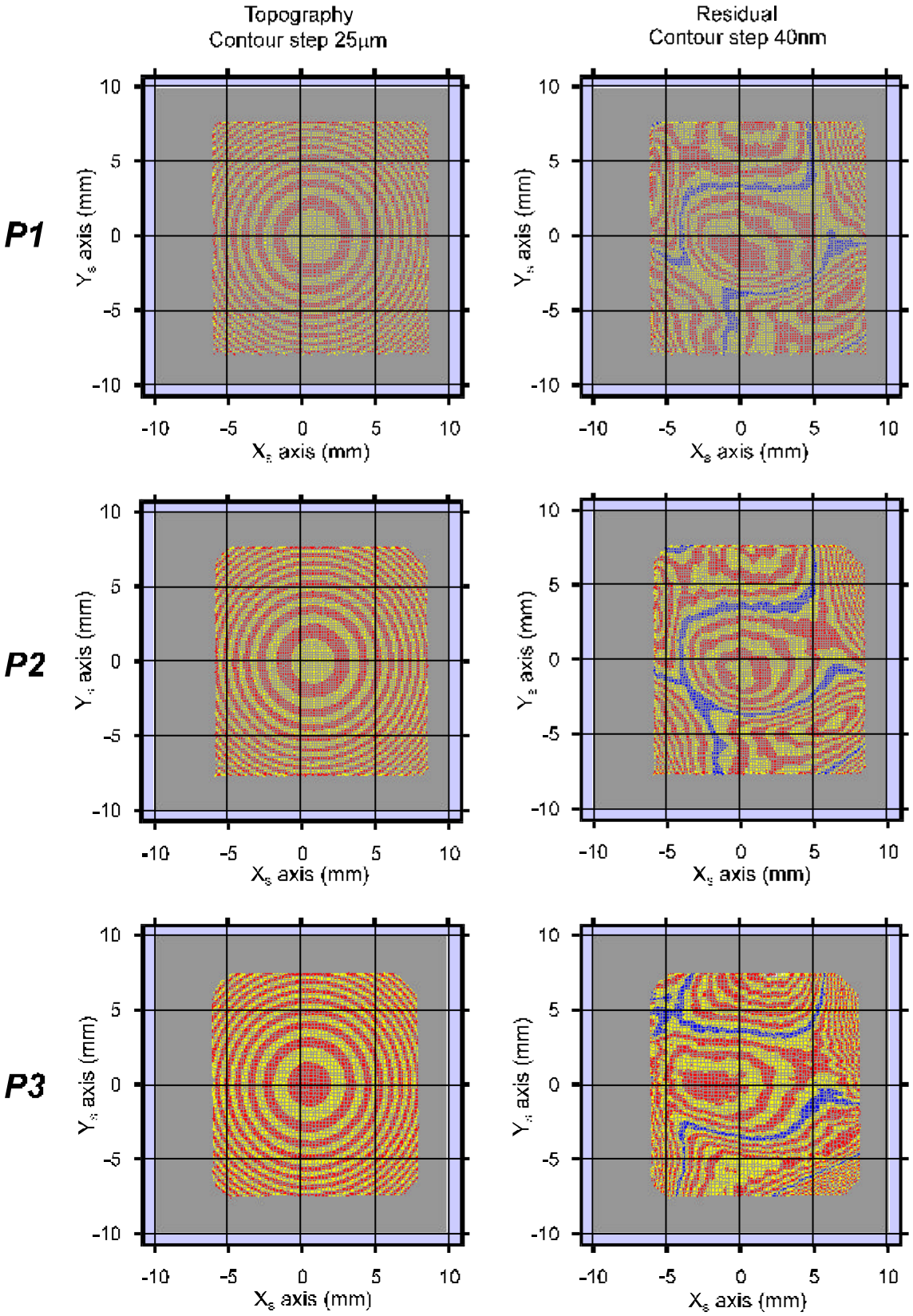

Table 6.3.5: Measured numerical results for sample P275A.

Sample P275A	Parameter	P1 d_R=180.8mm	P2 d_R=185.7mm	P3 d_R=193.3mm
Experiment	N(points)	7065	10228	15482
	Δz(mm)	0.401	0.368	0.321
	A(mm^2)	237.2	230.9	218.1
2D fitting	C_X(mm^{-1})	$6.240\ 10^{-3}$	$6.240\ 10^{-3}$	$6.236\ 10^{-3}$
	K_X(rad)	$-3.357\ 10^{-3}$	$-3.015\ 10^{-3}$	$-2.944\ 10^{-3}$
	r_x^2	0.999996	0.999994	0.999990
	C_Y(mm^{-1})	$6.239\ 10^{-3}$	$6.240\ 10^{-3}$	$6.233\ 10^{-3}$
	K_Y(rad)	$-2.218\ 10^{-3}$	$-1.909\ 10^{-3}$	$-1.732\ 10^{-3}$
	r_Y^2	0.99990	0.999986	0.999979
	R_X(mm)	160.26	160.25	160.37
	R_Y(mm)	160.30	160.26	160.44
3D fitting	R(mm)	160.14	160.16	160.34
	σ_R(mm)	$2.9\ 10^{-3}$	$2.3\ 10^{-3}$	$1.7\ 10^{-3}$
	x_0(mm)	0.5375	0.4826	0.4713
	σ_{Xo}(mm)	$5.3\ 10^{-5}$	$2.4\ 10^{-5}$	$2.9\ 10^{-5}$
	y_0(mm)	-0.3550	-0.3061	-0.2795
	σ_{Yo}(mm)	$4.9\ 10^{-5}$	$3.2\ 10^{-5}$	$2.7\ 10^{-5}$
	r^2	0.999998	0.999998	0.999998
	$\Delta z_{RESIDUAL}$(mm)	$5.146\ 10^{-4}$	$4.802\ 10^{-4}$	$5.056\ 10^{-4}$

Möller-Wedel radioscope reference measurement: R=160.2±0.1mm

Fig. 6.3.5: Measured surface topographies and residuals: sample P275A.

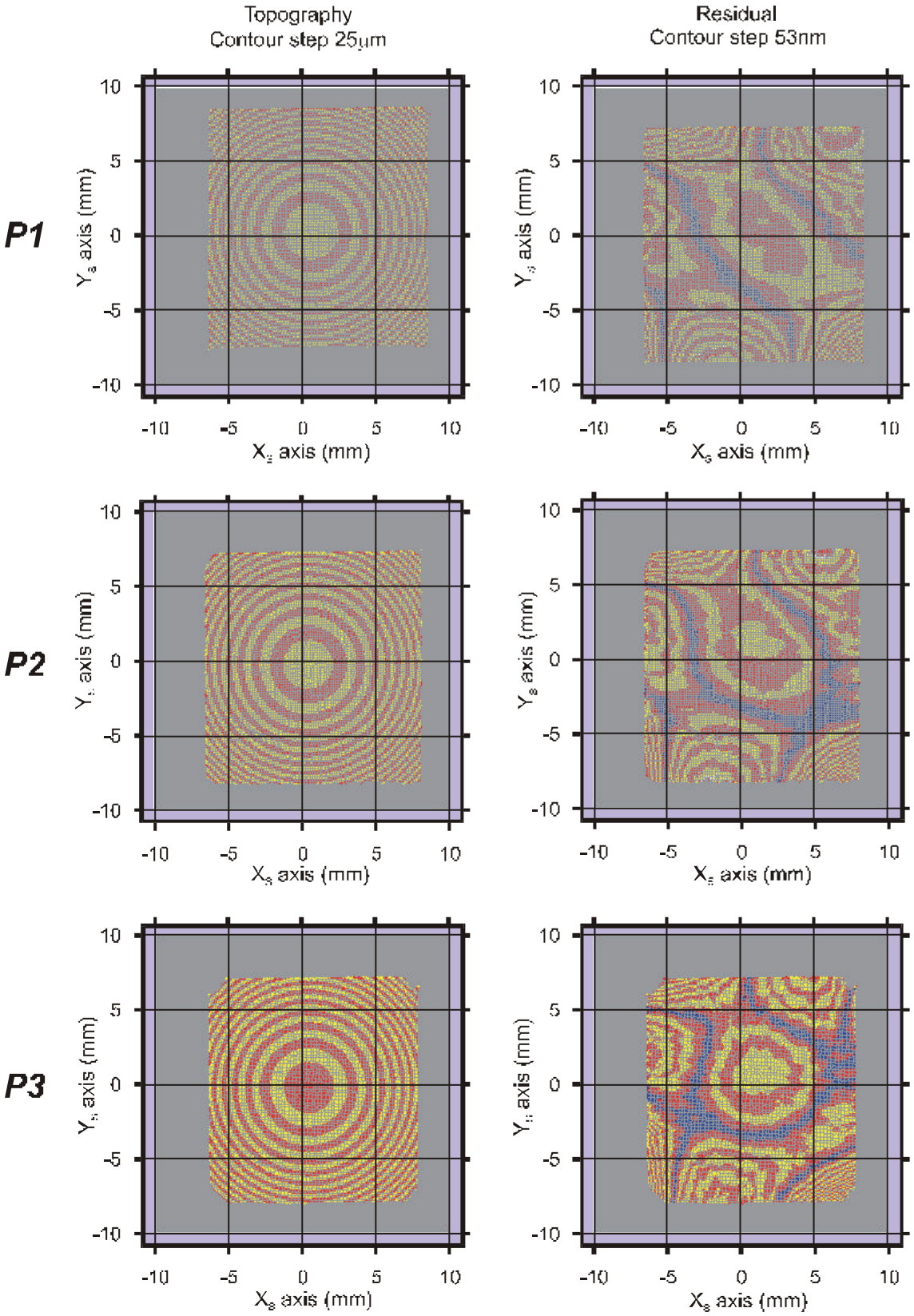

Table 6.3.6: Measured numerical results for sample P275B.

Sample P275B	Parameter	P1 d_R=180.8mm	P2 d_R=185.7mm	P3 d_R=193.3mm
Experiment	N(points)	6572	9532	14777
	Δz(mm)	0.396	0.349	0.327
	A(mm^2)	237.2	230.9	218.1
2D fitting	C_X(mm^{-1})	6.238 10^{-3}	6.234 10^{-3}	6.233 10^{-3}
	K_X(rad)	-4.085 10^{-3}	-2.122 10^{-3}	-3.918 10^{-3}
	r_x^2	0.999994	0.999994	0.999994
	C_Y(mm^{-1})	6.183 10^{-3}	6.177 10^{-3}	6.173 10^{-3}
	K_Y(rad)	1.728 10^{-3}	2.557 10^{-3}	2.228 10^{-3}
	r_Y^2	0.999995	0.999994	0.999994
	R_X(mm)	160.32	160.42	160.43
	R_Y(mm)	161.75	161.89	161.99
3D fitting	R(mm)	161.01	161.18	161.32
	σ_R(mm)	1.1 10^{-2}	9.7 10^{-3}	7.9 10^{-3}
	x_0(mm)	0.6537	0.3406	0.5945
	σ_{Xo}(mm)	2.0 10^{-4}	1.6 10^{-4}	1.4 10^{-4}
	y_0(mm)	0.2812	4.234 10^{-2}	0.4017
	σ_{Yo}(mm)	1.8 10^{-4}	3.275 10^{-5}	1.2 10^{-4}
	r^2	0.999970	0.999966	0.999968
	$\Delta z_{RESIDUAL}$(mm)	1.937 10^{-3}	1.915 10^{-3}	1.922 10^{-3}

Möller-Wedel radioscope reference measurement: R=161.0±0.1mm

Fig. 6.3.6: Measured surface topographies and residuals: sample P275B.

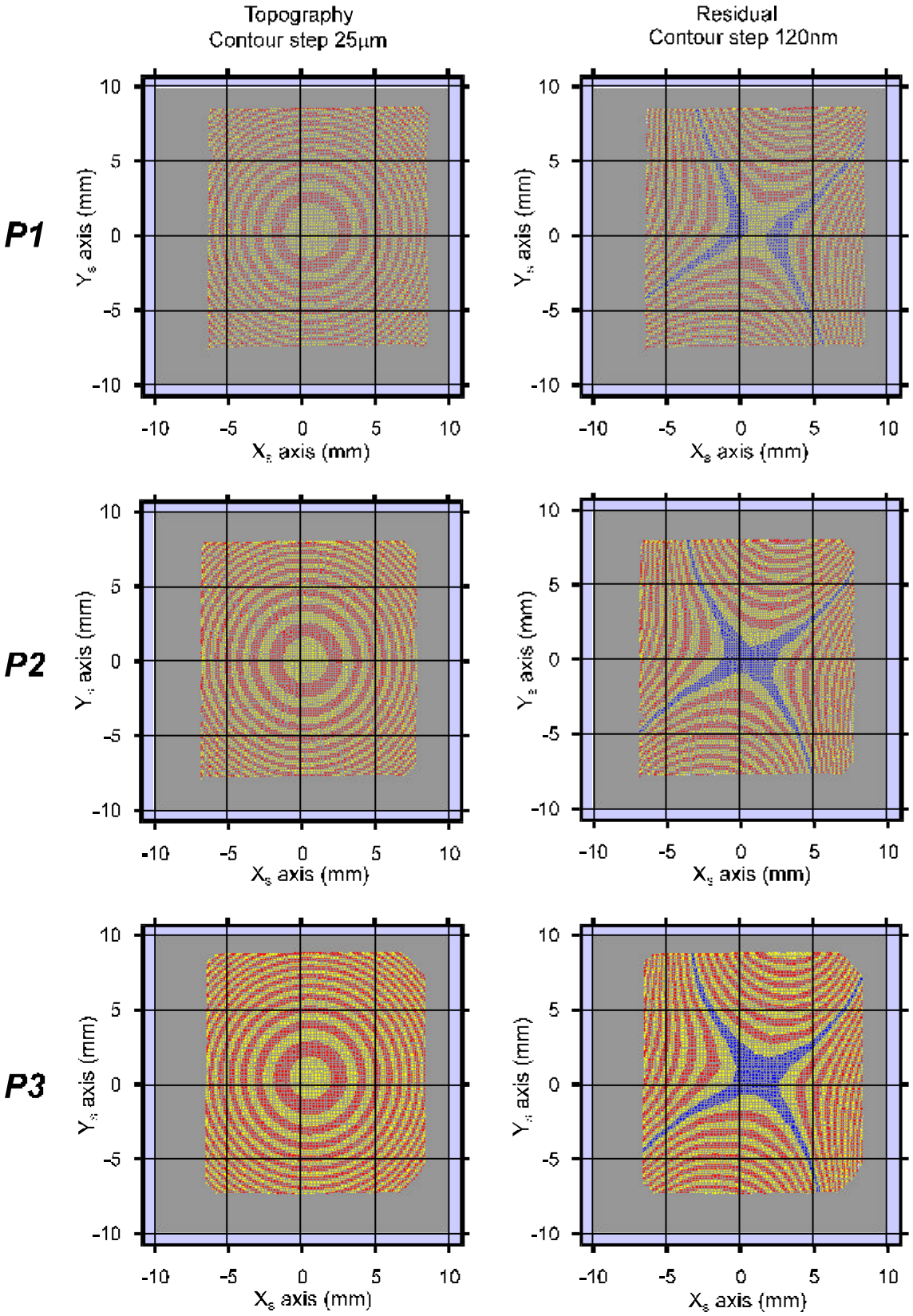

6.3.2.- Data analysis.

As a large amount of data has been put before the reader, we will point out the most remarkable tendencies that can be extracted from the experiments described. This is not intended to be an intensive commentary on the results obtained plot by plot, but a summary of some of the features shown in the obtained data. In particular, the influence of the increase of the d_R distance in the measurements will be studied.

A first conclusion may be drawn from the experimental parameters of the numerical results: as the d_R distance increases, the height variation and the sampled area of the lens decrease. This is an effect of the pupils of the system, which prevent some slopes on the reflected wavefront from reaching the CCD plane. As we are working in an out of focus configuration, when increasing the d_R distance the focusing point is also moved away from the pupils of the experimental setup, so the rays passing close to the limit of the field of view in short d_R distances will not go through the observation system for larger d_R distances, giving a smaller sampled area for longer d_R distances. We could sum this up by saying that the longer the d_R distance, the smaller the sample area with reflected rays not intersected by the pupils of the experimental setup.

The drop in height variation as the d_R distance increases is a logical consequence of the reduction in the sampled area of the surface. Another obvious consequence is the increase in the number of sampled points for larger d_R values, as more bright lines will appear in the ronchigram as the sample is moved away from the Ronchi ruling. The greater the number of bright lines, the greater the amount of data points available when the superposition of orthogonal eroded ronchigrams is performed.

The different height range in each measurement, combined with our previous decision to keep a fixed contour step for the data in one sample in all positions, is responsible for the progressive change of contour level that may be appreciated at the center of the topography or residual plots as the d_R distance is increased. A relative scale for each data item would provide more similar plots, but would entail greater difficulty in the comparison between data from each sample at different d_R distances.

We believe the high quality of the topographic measurements must be stressed, as no surface interpolation has been considered and each sampled point is yielding a given height in topographic measurements. This quality may be further confirmed by the correlation coefficients obtained in three-dimensional fitting procedures. In the residual

plots, deviations from the best-fit sphere may be seen to allow the repetitive measurements of submicrometric surface features.

The appearance of the residuals has a common pattern in positions P1, P2 and P3, in the six samples, demonstrating the repetitiveness of the topographies obtained under displacements of the sample surface. Only small deviations in the absolute measured values are introduced by surface displacements. However, the maximum height variation of the residual remains comparable in every position of the sample, with the reconstructed shape of the residual remaining qualitatively the same under displacement.

Another interesting feature is how nominally identical samples give different submicrometric surface residuals. These residuals from the best fit sphere of each sample may be grouped in three sets: samples P175A, P175B and P200A have a toroidally shaped residual, which in P200A and P175B has its axis placed along the X axis, and in P175A along the 30° direction from X axis, approximately; P200B and P275A residuals do not have higher deviations along one direction or another but instead present a general surface deformation; finally, sample P275B shows important residuals following a hyperboloidal shape, centered at the vertex of the surface. This behavior of the residuals coincides with what could be estimated from the test focusing in the radioscope, which followed comparable distortions in each of the samples. This means that the topographies obtained through the Ronchi test technique presented allow us to measure different topographies from surfaces which are presented as identical ones by the ophthalmic industry. However, the Ronchi test measurements also show that the radius of curvature of nominally identical surfaces is very similar, as this is the parameter usually controlled by the ophthalmic industry throughout the lens manufacturing process.

In fact, one of the most remarkable results obtained is the constancy of the measured radius of curvature throughout the three considered positions of the sample. Maximum variations in the measured radius of curvature values, both through two-dimensional and three-dimensional fitting, are always under 0.5mm, which, considering the radius of curvature values obtained, involve a deviation from the 0.3% of the measured value, well under the 2% uncertainty of the measurement calculated in Section 4.3.1. However, the results indicate a certain tendency to increase the radius of curvature values at larger d_R distances, although this increase stays around 0.3mm with all samples.

A relationship may be established between the fitted curvature results and the surface residuals of the samples. Notice how the group of surfaces with toroidal residuals presents different curvatures along the X and Y axes when using two-dimensional fitting, and how the radius of curvature value obtained through three-dimensional fitting is an intermediate value of those obtained through two-dimensional fitting, which is the behavior that one would expect from a slightly toroidal surface. Samples P200B and P275A display very similar curvatures along the X and Y axes, and the radius obtained through three-dimensional fitting is not always the intermediate value between the two curvatures obtained through two-dimensional fitting. In P275B, with its important curvature differences along the X and Y axes, the three-dimensional radius of curvature continues to be the intermediate value of the two radius of curvature obtained along the X and Y directions, as a consequence of the symmetry along the X and Y axes of the residual. The difference between the values of the two-dimensional fitted radius of curvature is 1.5mm in the P275B sample, the most significant in the samples presented. This big residual height agrees very well with the poorer (when compared to other samples) correlation coefficient of sample P275B, meaning the surface is the less spherical among the samples.

The independent term in two-dimensional fitting procedures, interpreted as the angular misalignment of the surface relative to the incident wavefront, and the position of the vertex of the surface in three-dimensional fitting procedures, are parameters whose values are affected by the displacement of the surface, sometimes changing sign, or with significantly varying values. This is an effect of the dependence of these parameters on the tilt and centering of the sample, which will obviously be dependent on the position of the sample surface. The remaining parameter from the fit, the correlation coefficient, is optimum in all cases, being only slightly worse in the abovementioned P275B case.

The comparison of the reference radius of curvature obtained through radioscopic measurements and the ones obtained through two-dimensional or three-dimensional curve-fitting is also very good. The radius of curvature obtained through three-dimensional fitting coincides with the radioscopic one slightly better than those obtained through two-dimensional fitting, because three-dimensional fitting and radioscopic measurements are overall measurements of the complete surface. Two-dimensional measurements focus on the curvature along one given direction, and, as

we have just shown in the case of the residual toricity of the samples, can take into account some directional effects of the residuals in the sample.

Standard deviations of the parameters and the range of surface height of the residuals vary in their behavior from one sample to another, but continue to have comparable values in all cases when varying the position of the surface. Although the number of data points increases as d_R increases, the quality of the fittings tends to drop slightly for long d_R distances, as may be seen in the small reductions of the correlation coefficients. Sample P275B, whose residuals are bigger than in any other sample, also shows standard deviations larger than those of any remaining sample

To sum up, we could say that the Ronchi test technique provides us with a robust tool for measuring radii of curvature and surface topographies of spherical surfaces, and by extension of rotationally symmetrical surfaces. Both two-dimensional and three-dimensional fitting techniques provide reliable results for the measurement of radii of curvature. While three-dimensional fitting provides a general radius of curvature value for the surface, and fits the reference radioscopic measurements better, two-dimensional fitting allows a qualitative prediction of the symmetry of the residuals from the best fit surface involved. The results in radii of curvature and surface topographies obtained remain nearly constant under displacement of the sample in the d_R range previously specified. Additional information in surface topographies is mostly obtained from the residual plots, which allow the measurement of submicrometric surface features. This makes possible to classify the surface deformation of the samples from the best fit sphere in toroidal, rotationally symmetrical and hyperboloidal geometries. Differences in the measured topographies of nominally identical lenses may be observed, although their radius of curvature values remain very similar.

All the foregoing data allows us to state that our experimental setup is fully calibrated, which was one of the main goals of this section, and has demonstrated that it is robust, reliable and independent of the position of the samples within the displacement ranges considered. The technique's potential in the measurement of rotationally symmetrical surfaces has been demonstrated, and our next goal will be to develop surface topographies and radius of curvature measurements in non-rotationally symmetrical surfaces.